However, real samples often contain low target-metal content, and the sensitivity of the existing MP-OES is low. The combination still poses challenges for MP-OES application in real sample analysis. Therefore, effective integration of MP-OES with efficient sample introduction methods is needed. The size of the existing MP-OES instrument can be further reduced, and its sensitivity can be enhanced when its sample introduction can be accomplished without a conventional sampling system (including a sampling pump, pneumatic nebulizer, or chemical vapor generator).

To solve these problems and improve analytical performance, the MP-OES has been coupled with many sample introduction techniques, including cold vapor generation,[22] hydride generation,[18] photochemical vapor generation,[23] tungsten coil (W-coil) electrothermal vaporization,[24, 25] and solid-phase microextraction (SPME).[21, 26-28] These sampling approaches can efficiently separate analytes from liquid phase as "dry" species before their exposure to microplasma, significantly enhancing the MP-OES sensitivity and alleviating matrix interferences. Among these methods, SPME is the most suitable for MP-OES because it can integrate the separation, preconcentration, and sample introduction of analytes from complex sample matrices into a single step.[29-31] This method simplifies sample pretreatment, which reduces the size of the MP-OES device and significantly improves its analytical performance. Zheng et al. first utilized the combination of SPME with MP-OES to achieve sensitive detection of lead and mercury.[26] However, conventional thermal desorption methods require additional temperature control and heat dissipation instrument modules. The resulting high energy consumption and larger device size limit instrument miniaturization. To address this issue, Wang et al. utilized a self-heating solid-phase microextraction (SH-SPME) device using gold-coated tungsten (Au@W) fibers for the in-situ determination of mercury in soil.[28] However, the gold coating only reacted with mercury; it could not be applied to determining other elements, and the tungsten substrate heated quickly and was not easy to control. Constructing a portable, integrated, low-power MP-OES device combined with SPME desorption technology remains challenging.

Therefore, this work aimed to develop a highly integrated, low power-consumption SH-SPME device and use it as the sampling unit in a palm-sized point discharge optical emission spectrometry (μPD-OES) device fabricated for the on-site detection of metals. The μPD-OES device uses a nozzle electrode as its discharge electrode, which allows complete excitation of the analyte and maintains long-term stable operation. Utilizing a nickel-chrome wire as the self-heating SPME fiber substrate, the thermal desorption of volatile analyte derivatives from the SPME fiber can be easily controlled and accomplished by directly heating the fiber with low power consumption. Furthermore, the developed self-heating SPME fiber eliminates the need for a conventional high-temperature thermal desorption chamber. We successfully integrated the battery power module, SPME sample introduction module, 3D-printed microplasma generation module, and data processing module into a palm-sized device (20.3 cm length × 10.3 cm width × 10.5 cm height). The device features low power consumption (~25 W) driven by an integrated battery, low gas consumption (60 mL min^{-1}), and high sensitivity. It ran continuously for 4 h in practical tests and was successfully applied to detect lead in human urine and hair. To our knowledge, this is the first report of coupling an SH-SPME unit with a highly integrated handheld μPD-OES device for on-site analysis of elements other than mercury. The device shows great potential for monitoring elemental exposure in remote areas and expanding its application to determining other elements. It provides a new tool for rapid response and field analysis of public health events and environmental pollution incidents.

EXPERIMENTAL

Fabrication of the handheld μPD-OES device. As shown in Fig. 1a, the handheld μPD-OES device consists of a sample introduction unit and a microplasma excitation chamber (Fig. 1b), a miniature charge-coupled device (CCD), a microcomputer board for data processing, a power supply, and a 3D-printed polylactic acid (PLA) shell. The customized setup comprised a sample introduction unit, thermal desorption chamber, and microplasma generation chamber, which were integrated into a machined polytetrafluoroethylene (PTFE) unit (25 × 20 × 60 mm). Similar to a gas chromatograph (GC) injector, a small hole (1.5 mm) was drilled to allow the insertion of the SPME fiber and a PTFE cap and GC injection septum were applied to ensure that the chamber was airtight. The other end of the PTFE tube was connected to a desorption chamber. The lower end of the thermal desorption chamber was linked to a 3D-printed discharge chamber. A high voltage was applied via a customized booster to a metal nozzle and tungsten rod on the other side of the discharge chamber, allowing the microplasma to be easily generated and maintained in an argon gas atmosphere. The optical emission from the discharge passed through a quartz window (10 × 10 × 1 mm) located on the surface of the discharge chamber and was captured using a handheld CCD spectrometer (Ocean ST, spectral range 185–506 nm, Ocean Optics Inc., Dunedin, FL). The spectrometer was equipped with a 74-DA direct-attach collimating lens (10 mm focal length, Ocean Optics, Inc., USA) to capture microplasma excitation signals and concentrate them onto the spectrometer slit. The read, processed spectrometer data display was achieved via a 5.5-inch screen (Hinde Electronics) embedded on the device and connected via two USB ports. The power supply module primarily operated through a multichannel power control panel that divided a 12 V 12000 mAh lithium battery (Delipow) into three non-interfering circuits to provide power for the microcomputer (Intel M1K),

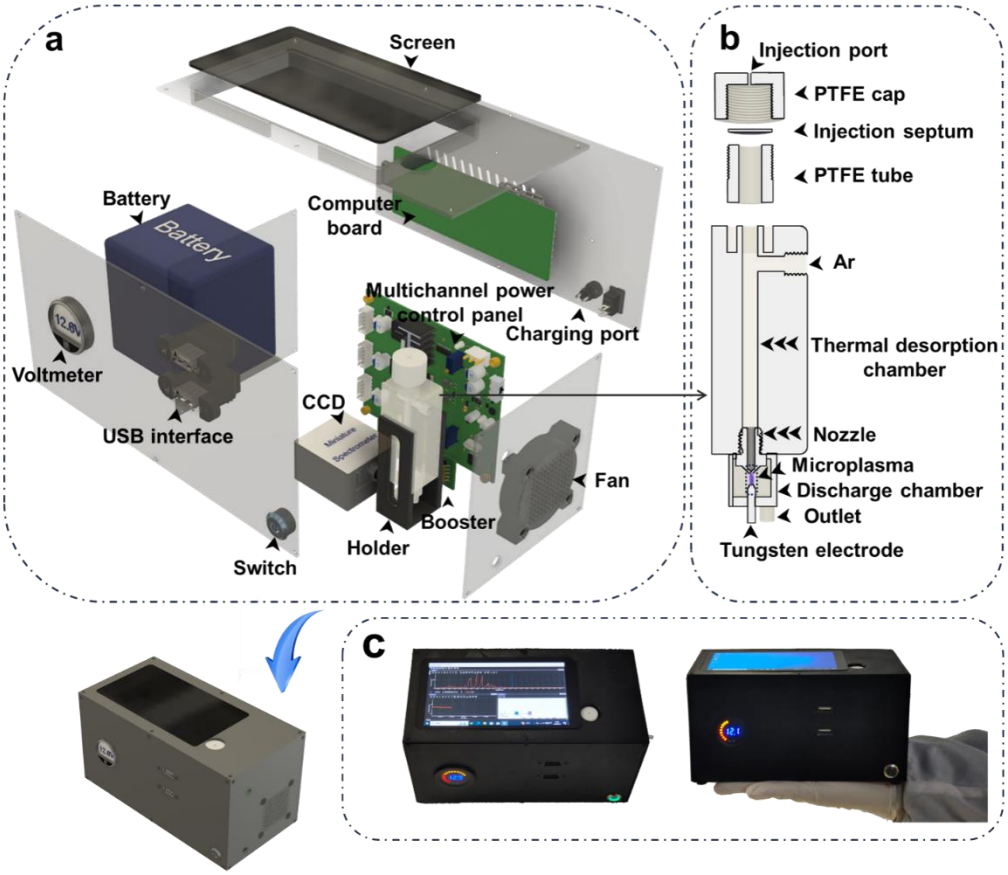

Fig. 1 (a) Schematic diagram of μPD-OES structure and (b) details of introduction module and discharge chamber. (c) Physical drawing of device.

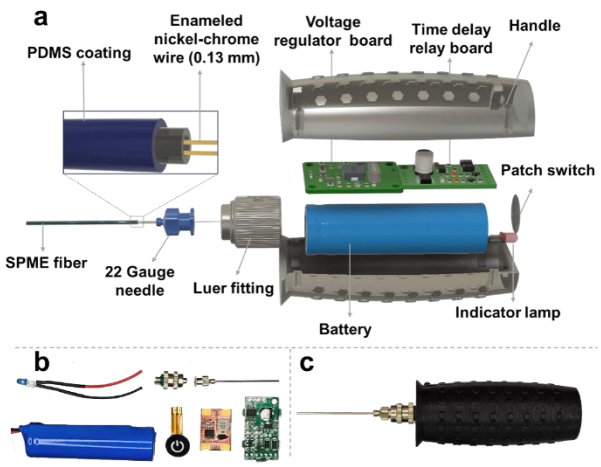

Fig. 2 (a) Schematic diagram of the SH-SPME unit structure; (b) SH-SPME component; (c) physical drawing of the handle.

excitation source, and cooling fan, which enabled the entire device to run for 4 h. The designed cooling fan effectively dissipated the instrument-generated heat during operation (Fig. S1). A digital voltmeter (Hongtefa Technology Co.) was used to monitor battery voltage in real-time. The entire machine was approximately the size of a palm (20.3 cm length × 10.3 cm width × 10.5 cm height), as shown in Fig. 1c. The device details are shown in Figs. S2-S5.

Fabrication of the SH-SPME device. As shown in Fig. 2a, the designed SPME fiber was a 22G needle (length 50 ×i. d. 0.41 × o. d. 0.71 mm) loaded with an enameled nickel-chrome wire (14 cm in length, 0.13 mm in diameter) to form a closed loop with the voltage regulator circuit board, which was connected to the handle through a Luer fitting. As shown in Fig. 2b, the self-heating unit integrated a battery, indicator lamp, and patch switch. A voltage regulator board was utilized to maintain a constant operating voltage, preventing deterioration of the desorption performance caused by the battery voltage drop during operation. To control the temperature and desorption time, a time-delayed relay board that worked with a voltage regulator circuit board was designed to ensure system stability and control. An LED light indicated the device operational status when a patch switch was pressed. All the above components were integrated and assembled into a 3D- printed

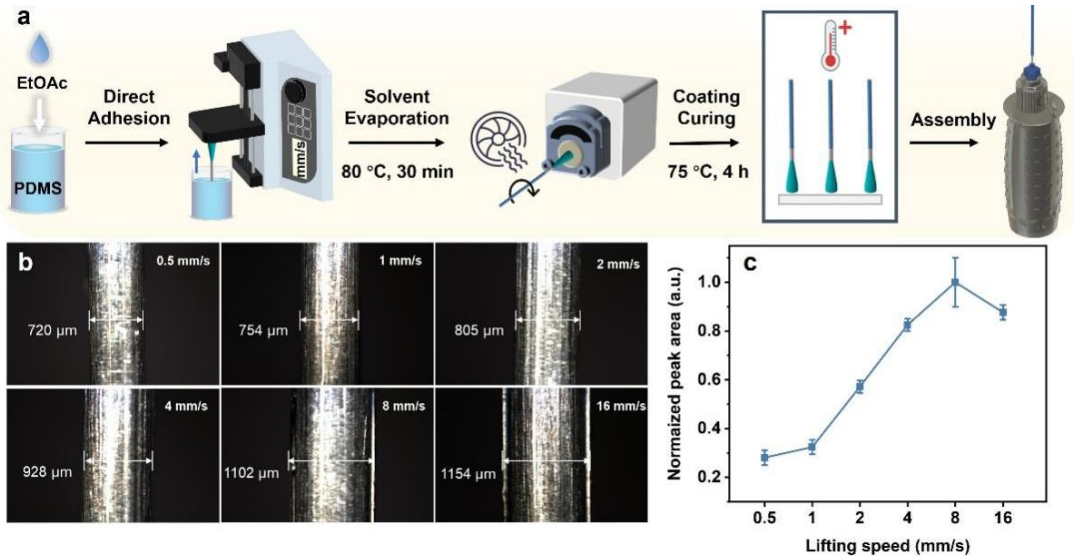

Fig. 3 (a) Schematic diagram of SPME fiber preparation; (b) 3D digital microscope images of PDMS fiber; (c) effect of coating lifting speed on lead responses.

handle (PLA material) with an ergonomically designed structure and non-slip-textured surface (Fig. 2c). A single 18650 lithium battery powered the entire SH-SPME device, and the details of the time-delayed relay board are shown in Fig. S6.

Coating preparation. Before preparation, the needle was polished with 200 mesh sandpaper, cleaned ultrasonically in deionized water, methanol, and acetone for 30 min, and dried at room temperature. As shown in Fig. 3a, PDMS was mixed with the curing agent at a ratio of 10:1, and ethyl acetate was added at a volume ratio of 5:1, followed by stirring under vacuum for 30 min. The needle was then fixed onto a vertical syringe pump, and a constant pump speed was set to lift the needle consistently and steadily to prepare the coating. The pump speed was set to rotate the fibers consistently (90 rpm), and a hair dryer was used to accelerate solvent evaporation. After the PDMS solidified, the needles were placed in an oven for 4 h for further solidification, and an enameled nickel-chrome wire was folded and inserted into the needle to complete the unit assembly.

Analytical procedure. Five milliliters of the lead standard or pretreated sample solution (The digestion procedure is outlined in Table S1), 1 mL of HAc-NaAc buffer (pH 4.5), and 3.8 mL deionized water were placed in a 40 mL brown glass vial. Subsequently, the prepared SPME fibers were inserted into the vial headspace, which was immediately sealed with a PTFE-coated silicone rubber septum. A 200 μL 1% (w/v) solution of tetraethylborate ($NaBEt_4$) was rapidly injected into the sample solution, and the mixture was stirred at 1200 rpm (room temperature) for 12 min to generate tetraethyl lead for extraction by the SPME fiber. After the extraction, the SH-SPME unit was transferred to the desorption chamber. The extracted tetraethyl lead was released from the SPME fibers through the self-heating function and introduced into the discharge chamber for μPD-OES detection.

RESULTS AND DISCUSSION

Feasibility of SH-SPME-μPD-OES for lead detection. SPME integrates the analyte sampling, separation, and preconcentration from complex sample matrices and eliminates the conventionally used sample introduction system when coupled with atomic spectroscopy. Therefore, using SPME as a sample introduction method can significantly improve the analytical performance of MP-OES and reduce its spectrometer size. Although SH-SPME has been used previously as an efficient MP-OES sampling technique, the SPME fiber in that instance was coated with gold and was only effective for preconcentrating mercury. To validate the feasibility of integrating a customized SH-SPME unit with handheld μPD-OES for analysis, a 40 μg L^{-1} standard solution of lead was tested to evaluate its performance. The analytical results, as shown in Fig. 4a, demonstrate that the characteristic atomic emission lines of lead (261.4, 283.3, 363.9, 368.3, and 405.8 nm)[26] can be easily distinguished from the background emission of the argon microplasma, confirming the feasibility of determining lead by the integration of SH-SPME unit with handheld μPD-OES device. Because the characteristic emission lines of lead overlap with those of the background OH (283 nm) and Ar (405.8 nm), 368.3 nm was chosen as the typical emission line for lead. To improve the accuracy and stability of the collected analytical characteristic emission spectra of lead, a background correction method was used to simultaneously record the response of lead at

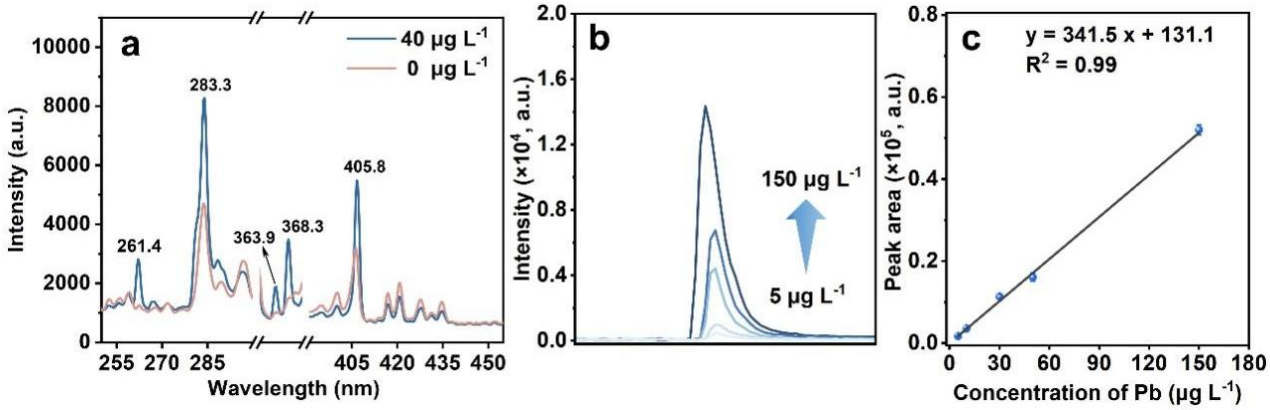

Fig. 4 (a) Optical emission spectra of 40 μg L^{-1} of lead and blank by SH-SPME-μPD-OES; (b) plots of lead atomic emission intensity from 5 to 150 μg L^{-1} and (c) calibration curve established by SH-SPME-μPD-OES.

368.3 nm as well as the background emission intensity at 369.8 nm.[32]

Optimization of SH-SPME. According to previous studies,[26,28] the extraction capacity, retention time, and desorption efficiency of the analyte are significantly affected by the thickness of the SPME fiber coating. Therefore, the effect of PDMS coating thickness on lead extraction was carefully investigated. PDMS coatings of various thicknesses could be prepared by changing the speed at which the SPME fiber was pulled from the PDMS solutions.[33] As shown in Fig. 3c, the obtained lead responses increased as the fiber lifting speed increased from 0.5 to 8 mm s^{-1}; then, at higher speeds, the responses decreased again. A lower lifting speed led to a thin coating, facilitating heat transfer and rapid analyte desorption from the SPME fiber. However, a thin coating caused low adsorption capacity and low response; a higher lifting speed rendered the coating too thick to release the analyte efficiently from the fiber, also leading to a low response. Consequently, a lifting speed of 8 mm s^{-1} was selected. The thickness of the PDMS coating, calculated by subtracting the bare needle diameter (710 μm) from the measured thickness (1102 μm), was 196 μm.

The voltage determines the desorption temperature and significantly affects the response and peak shape of the analyte. Thus, its effect on the desorption efficiency of lead was studied, and the analytical results are shown in Fig. S7. When the test voltage increases from 4.5 to 7.5 V, the obtained signals gradually change from an asymmetrical flat, low peak to a slender, symmetrical peak, while the complete desorption time is dramatically shortened from about 40 to 12 s. This can be explained by the fact that a higher voltage induces the enameled nickel-chromium wire to heat up faster and reach a higher temperature, thus realizing rapid, efficient analyte desorption. To protect the insulating coating of the enameled nickel-chrome wire from excessive voltage that would cause the heating wire to fuse and damage the PDMS coating,[29] a higher voltage (7.5 V, which generated a 210 °C desorption temperature) was chosen as the optimal desorption voltage. The desorption power is only 2.5 W. To improve the SH-SPME extraction performance using the prepared fiber, the sample solution pH value, stirring speed, derivatization reagent amount, and extraction time were further optimized (Fig. S8); pH 4.5 HAc/NaAc buffer solution, 1200 rpm stirring speed, 0.02% (m/v) derivatization reagent concentration, and 12 min extraction time were used for subsequent experiments.

Optimization of operation parameters of handheld μPD-OES. The experimental parameters affecting μPD-OES were carefully investigated to obtain the maximum response from this highly integrated device, including the electrode nozzle diameter, discharge gap, and argon discharge gas flow rate. The analytical results are presented in Fig. S9. Based on these results, a nozzle diameter of 0.6 mm, 3 mm of electrode distance, and 60 mL min^{-1} of argon flow rate were used.

Interferences. The effects of various common ions on lead detection were investigated, including Na^+, K^+, Ca^{2+}, Mg^{2+}, Zn^{2+}, Cd^{2+}, Sn^{2+}, and Hg^{2+}. As shown in Table S2, no significant interference from Na^+, K^+, Ca^{2+}, Mg^{2+}, and Zn^{2+} is observed even at their concentrations as high as 100 mg L^{-1}. Although Cd^{2+}, Sn^{2+}, and Hg^{2+} influence on lead response beyond 2 mg L^{-1}, the effect of 100-fold Cd^{2+}, 50-fold Sn^{2+}, and 20-fold Hg^{2+} on lead response is not obvious. The above-mentioned results suggest that the designed SH-SPME-μPD-OES device exhibits excellent anti-interference capability and ability to identify the target elements based on their characteristic emissions.

Analytical figures of merit. The analytical performance of the SH-SPME-μPD-OES was evaluated under optimal experimental conditions. Fig. 4b and 4c show a linear dynamic range from 5 to

Table 1. Comparison of the proposed device with other atomic spectroscopic methods for lead determination

Analysis method	Battery-operated	Data processing system	LOD, μg L^{-1}	Ref.
ETV-PD-OES	-	-	8.0	[35]
EMV-DC-APGD-AES	-	-	30.8	[36]
SCGD-OES	√	-	23.0	[37]
FLA-APGD-OES	-	-	1.7	[38]
LLE-MP-AES	-	-	4.2	[39]
IG-DBD-OES	-	-	0.6	[40]
EE-DBD-OES	-	-	4.5	[41]
SPME-OES	-	-	0.003	[26]
This work	√	√	1.2	-

ETV: electrothermal vaporizer; PD: point discharge; EMV: electromagnetic heating vaporization; DC: direct current; APGD: atmospheric pressure glow discharge; AES: atomic emission spectrometry; SCGD: solution cathode glow discharge; FLA: flowing liquid anode; LLE: liquid-liquid extraction; MP: microwave-induced plasma; IG: insert-and-go; DBD: dielectric barrier discharge; EE: electroextraction.

Table 2. Analytical results of lead determination in CRMs by SH-SPME-μPD-OES

CRMs	Certified, μg L^{-1}	Detected,[a] μg L^{-1}	t-test
GBW09104	101.0 ± 12.0	106.3 ± 11.5	0.82
GBW09105	308.0 ± 32.0	304.6 ± 28.2	0.25

[a] Mean and standard deviation of results ($t_{0.05,2}$ = 4.30; P = 95%; n = 3).

Table 3. Analytical results from actual urine samples by SH-SPME-μPD-OES

Sample	Added, μg L^{-1}	Found,[a] μg L^{-1}	Recovery, %
Urine 1	0	ND[b]	-
	5	4.6 ± 0.2	92
	100	108.1 ± 6.6	108
Urine 2	0	ND[b]	-
	5	4.8 ± 0.3	96
	100	102.4 ± 3.5	102

[a] Mean and standard deviation of results (n=3); [b] not detected.

Table 4. Analytical results in actual hair samples by ICP–MS and SH-SPME-μPD-OES

Sample	ICP-MS, mg kg^{-1}	SH-SPME-μPD-OES,[a] mg kg^{-1}	t-test
Hair 1	1.27 ± 0.16	1.20 ± 0.13	0.19
Hair 2	1.32 ± 0.14	1.34 ± 0.09	0.21
Hair 3	2.68 ± 0.21	2.52 ± 0.17	0.26

[a] Mean and standard deviation of results ($t_{0.05,4}$ = 2.78; P = 95%; n = 3).

150 μg L^{-1} with good linear correlation (R^2>0.99). The limit of detection (LOD), calculated according to the formula 3σ/k with 11 measurements of a blank solution, where σ is the standard deviation and k is the slope of the calibration curve, was 1.2 μg L^{-1}. The enhancement factor (EF), defined as the slope of the standard curve with an enrichment step divided by that obtained without analyte preconcentration, is 83.3 (Fig. S10), indicating that the sensitivity of the proposed method on lead detection is greatly improved. The analytical performance of SH-SPME-μPD-OES and other MP-OES-based methods for determining lead is summarized in Table 1. Owing to the advantages of pre-concentration and the elimination of matrix interference offered by SH-SPME, the LOD obtained by this handheld spectrometer is comparable to or better than that of most existing MP-OES methods. Notably, this is the first highly integrated spectrometer that assembles SPME desorption and analytical detection of elements, data collection, and result reading, offering significant advantages for field analysis. To further validate the stability of the SPME fiber, 40 extraction cycles were performed on the fiber, and a relative standard deviation (RSD) of 4.5% was obtained (Fig. S11), which indicated good repeatability and stability. To assess the precision and reproducibility of the proposed system, five duplicate standard solutions containing 10 μg L^{-1} of lead were measured under the same conditions. An RSD of 4.7% was obtained, as shown in Fig. S12. Notably, the proposed handheld device could be operated continuously and stably for 4 h using a 12000 mAh battery.

Application of SH-SPME-μPD-OES for on-site analysis. The accuracy of the developed device was verified by analyzing two urinary CRMs and two real urine samples collected from volunteers. The analytical results are summarized in Tables 2 and 3. The t-test showed no significant difference between the obtained analytical results and the certified values at the 95% confidence level. As can be seen from Table 3, no lead could be detected in the two real urine samples because their endogenous concentrations were lower than the LOD. Their recoveries of spiked lead (5 μg L^{-1} and 100 μg L^{-1}) were tested, leading to recoveries ranging from 92 to 108% for these samples. These analytical results demonstrate the accuracy of the proposed SH-SPME-μPD-OES system. To validate the feasibility and practicability of the SH-SPME-μPD-OES on accurate lead detection in other biological samples, three actual hair samples were analyzed by the proposed method and ICP-MS after their microwave-assisted digestion. As shown in Table 4, the analytical results obtained by the proposed method agree well with those obtained by ICP-MS at the 95% confidence level, further confirming the practicality of the SH-SPME-μPD-OES for lead analysis in a complex matrix.

CONCLUSION

This study successfully used a handheld microplasma atomic emission spectrometer equipped with an SH-SPME device for lead detection. This highly integrated device assembles sampling, detection, and data processing systems, enabling the rapid on-site detection of heavy metals. The SH-SPME device, characterized by its low power consumption, was coupled with battery-powered handheld μPD-OES. It can work continuously for 4 h, meeting the practical operational requirements of field analytical chemistry. The development of this device marks a significant breakthrough in the miniaturization of atomic spectroscopy analyzers, enhancing the efficiency and convenience of on-site detection and expanding its application prospects in various fields such as environmental monitoring, food safety, and medical health. The device demonstrates great potential for rapidly screening and detecting heavy metals. It is particularly suitable for emergency responses to environmental pollution incidents and health examinations in remote areas, providing a convenient, efficient on-site analysis solution for related fields.

ASSOCIATED CONTENT

The supporting information (Tables S1-S2 and Figs. S1-S12) is available at www.at-spectrosc.com/as/home

AUTHOR INFORMATION

Chengbin Zheng is currently a professor of environmental analytical chemistry in the College of Chemistry of Sichuan University. He received his B.S. and Ph.D. degrees from Sichuan University and successively worked as a postdoctoral researcher at the National Research Council Canada and the Research Center for Eco-Environmental Science, Chinese Academy of Sciences. His current research focuses on the development of field analytical methods and instruments for environmental analysis. He has been working as editorial board of *Atomic Spectroscopy*.

Yurong Deng is currently a lecturer in the College of Chemistry of Sichuan University. She received her B.S. and M.S. degrees from Sichuan University and her Ph.D. degree from the University of New Mexico, USA. Her current research interests are focused on scientific issues in environmental analysis, developing new methods for field analysis, and addressing environmental pollution problems.

Corresponding Author

*C. B. Zheng

Email address: abinscu@scu.edu.cn

*Y. R. Deng

Email address: ydeng@scu.edu.cn

Notes

The authors declare no competing financial interest.

ACKNOWLEDGMENTS

The authors gratefully thank the National Nature Science Foundation of China (No. 22076128) for financial support of this work.

REFERENCES

1. P. Pohl and R. E. Sturgeon, *Trac-Trends Anal. Chem.*, 2010, **29**, 1376-1389. https://doi.org/10.1016/j.trac.2010.07.015
2. R. Clough, C. F. Harrington, S. J. Hill, Y. Madrid, and J. F. Tyson, *J. Anal. At. Spectrom.*, 2023, **38**, 1339-1371. https://doi.org/10.1039/D3JA90022C
3. E. H. Evans, J. Pisonero, C. M. M. Smith, and R. N. Taylor, *J. Anal. At. Spectrom.*, 2023, **38**, 974-999. https://doi.org/10.1039/D3JA90013D
4. L. Husáková, I. Urbanová, M. Šafránková, and T. Šídová, *Talanta*, 2017, **175**, 93-100. https://doi.org/10.1016/j.talanta.2017.07.031
5. X. Liu, Z. Zhu, H. Li, D. He, Y. Li, H. Zheng, Y. Gan, Y. Li, N. S. Belshaw, and S. Hu, *Anal. Chem.*, 2017, **89**, 6827-6833. https://doi.org/10.1021/acs.analchem.7b01255
6. G. Yang, H. Tazoe, and M. Yamada, *Anal. Chim. Acta*, 2018, **1008**, 66-73. https://doi.org/10.1016/j.aca.2017.12.049
7. J. Wei, Y. Su, Y. Lin, Y. Luo, Y. Li, Y. Deng, and C. Zheng, *Anal. Chem.*, 2023, **95**, 7409-7415. https://doi.org/10.1021/acs.analchem.3c00389
8. N. Altunay and M. Tuzen, *Food Chem.*, 2021, **364**, 130371. https://doi.org/10.1016/j.foodchem.2021.130371
9. J. J. López-Mayán, B. Álvarez-Fernández, E. Peña-Vázquez, M. C. Barciela-Alonso, A. Moreda-Piñeiro, and P. Bermejo-Barrera, *Talanta*, 2022, **247**, 123556. https://doi.org/10.1016/j.talanta.2022.123556
10. J. Jing, S. He, J. Yang, R. Yang, Y. Lin, and C. Zheng, *Food Chem.*, 2023, **406**, 135077. https://doi.org/10.1016/j.foodchem.2022.135077
11. P. Almerud, G. Zamaratskaia, A. K. Lindroos, H. Bjermo, E. M. Andersson, T. Lundh, E. H. Ankarberg, and S. Lignell, *Environ. Res.*, 2021, **197**, 110991. https://doi.org/10.1016/j.envres.2021.110991
12. C. Wu, X. Wei, X. Men, X. Zhang, Y.-L. Yu, Z.-R. Xu, M.-L. Chen, and J.-H. Wang, *Anal. Chem.*, 2021, **93**, 8203-8209. https://doi.org/10.1021/acs.analchem.1c00484

13. X. Zhang, S. Liu, X. Wei, Y.-L. Yu, and J.-H. Wang, *Anal. Chem.*, 2021, **93**, 10577-10583. https://doi.org/10.1021/acs.analchem.1c01745
14. Y. Li, P. Chen, Y. Su, T. Ren, Y. Deng, Y. Lin, and C. Zheng, *Sens. Actuator B-Chem.*, 2023, **395**, 134534. https://doi.org/10.1016/j.snb.2023.134534
15. Z. Shu, H. Luo, P. Mengting, T. Yunfei, X. Hou, J. Xiaoming, and C. Zheng, *Anal. Chem.*, 2015, **87**, 10712-10718. https://doi.org/10.1021/acs.analchem.5b02820
16. L. An-Qin, T. Yunfei, W. Mingji, W. Li, X. Kailai, X. Hou, and C. Zheng, *Chin. Chem. Lett.*, 2017, **28**, 189-196. https://doi.org/10.1016/j.cclet.2016.06.056
17. Z. Shu, T. Yunfei, H. Yin, S. Yubin, W. Li, X. Hou, and C. Zheng, *Environ. Sci. Technol.*, 2017, **51**, 9109-9117. https://doi.org/10.1021/acs.est.7b01064
18. L. He, Y. Lin, P. Chen, Y. Su, Y. Li, and C. Zheng, *J. Hazard. Mater.*, 2022, **439**, 129607. https://doi.org/10.1016/j.jhazmat.2022.129607
19. Y. Liqing, Y. Wenhui, Y. Rui, W. Yuke, P. Zhengqin, W. Xi, H. Ke, L. Hong, Z. Jinyi, and Z. Chengbin, *Talanta*, 2024, **272**, 125833. https://doi.org/10.1016/j.talanta.2024.125833
20. H. Liangbo, L. Yao, S. Yubin, L. Yuanyuan, D. Yurong, and C. Zheng, *Anal. Chem*., 2022, **94**, 17514-17521. https://doi.org/10.1021/acs.analchem.2c03784
21. R. Yang, Y. Lin, J. Yang, L. He, Y. Tian, X. Hou, and C. Zheng, *Anal. Chem*., 2021, **93**, 6972-6979. https://doi.org/10.1021/acs.analchem.0c05254
22. R. Rong, Z. Cai, X. Li, and Z. Wang, *J. Anal. At. Spectrom.*, 2022, **37**, 2377-2382. https://doi.org/10.1039/D2JA00257D
23. Y. Su, Y. Lin, Y. Li, T. Ren, Y. Deng, and C. Zheng, *Anal. Chim. Acta*, 2023, **1261**, 341184. https://doi.org/10.1016/j.aca.2023.341184
24. N. Li, Z. Wu, Y. Wang, J. Zhang, X. Zhang, H. Zhang, W. Wu, J. Gao, and J. Jiang, *Anal. Chem.*, 2017, **89**, 2205-2210. https://doi.org/10.1021/acs.analchem.6b03523
25. X. Jiang, Y. Chen, C. Zheng, and X. Hou, *Anal. Chem.*, 2014, **86**, 5220-5224. https://doi.org/10.1021/ac500637p
26. C. Zheng, L. Hu, X. Hou, B. He, and G. Jiang, *Anal. Chem.*, 2018, **90**, 3683-3691. https://doi.org/10.1021/acs.analchem.7b04759
27. Z. He, Y. Lin, Y. Wang, L. He, X. Hou, and C. Zheng, *Anal. Chem.*, 2020, **92**, 9583-9590. https://doi.org/10.1021/acs.analchem.0c00755
28. Y. Wang, Y. Lin, T. Ren, Y. Yang, Z. He, Y. Deng, and C. Zheng, *Anal. Chem.*, 2023, **95**, 10873-10878. https://doi.org/10.1021/acs.analchem.3c00686
29. C. L. Arthur and J. Pawliszyn, *Anal. Chem.*, 1990, **62**, 2145-2148. https://doi.org/10.1021/ac00218a019
30. N. Reyes-Garcés, E. Gionfriddo, G. A. Gómez-Ríos, M. N. Alam, E. Boyacı, B. Bojko, V. Singh, J. Grandy, and J. Pawliszyn, *Anal. Chem.*, 2018, **90**, 302-360. https://doi.org/10.1021/acs.analchem.7b04502
31. É. A. Souza-Silva, R. Jiang, A. Rodríguez-Lafuente, E. Gionfriddo, and J. Pawliszyn, *Trac-Trends Anal. Chem.*, 2015, **71**, 224-235. https://doi.org/10.1016/j.trac.2015.04.016
32. Y. Yu, Z. Du, M. Chen, and J. Wang, *Angew. Chem.-Int. Edit.*, 2008, **47**, 7909-7912. https://doi.org/10.1002/anie.200802681
33. L. E. Scriven, *MRS Online Proceedings Library*, 1988, **121**, 717-729. https://doi.org/10.1557/PROC-121-717
34. G. Camino, S. M. Lomakin, and M. Lazzari, *Polymer*, 2001, **42**, 2395-2402. https://doi.org/10.1016/S0032-3861(00)00652-2
35. Y. Deng, J. Hu, M. Li, L. He, K. Li, X. Hou, and X. Jiang, *Anal. Chim. Acta*, 2021, **1163**, 338502. https://doi.org/10.1016/j.aca.2021.338502
36. Z. Cai, L. Qian, X. Peng, and Z. Wang, *Anal. Chem.*, 2021, **93**, 14701-14707. https://doi.org/10.1021/acs.analchem.1c03057
37. X. Peng, X. Guo, F. Ge, and Z. Wang, *J. Anal. At. Spectrom*., 2019, **34**, 394-400. https://doi.org/10.1039/C8JA00369F
38. K. Greda, K. Swiderski, P. Jamroz, and P. Pohl, *Anal. Chem.*, 2016, **88**, 8812-8820. https://doi.org/10.1021/acs.analchem.6b02250
39. S. V. Smirnova, T. O. Samarina, D. V. Ilin, and I. V. Pletnev, *Anal. Chem.*, 2018, **90**, 6323-6331. https://doi.org/10.1021/acs.analchem.8b01136
40. S. Liu, X.-X. Xue, Y.-L. Yu, and J.-H. Wang, *Anal. Chem.*, 2021, **93**, 6262-6269. https://doi.org/10.1021/acs.analchem.1c00819
41. S. Liu, H. Shen, C. Gao, J.-H. Liu, Y.-L. Yu, and J.-H. Wang, *Anal. Chim. Acta*, 2022, **1232**, 340497. https://doi.org/10.1016/j.aca.2022.340497